JCB Journal of Cell Biology

ARTICLE

PLK1 plays dual roles in centralspindlin regulation during cytokinesis

Ingrid E. Adriaans[1,2], Angika Basant[3], Bas Ponsioen[1,2], Michael Glotzer[3], and Susanne M.A. Lens[1,2]

Cytokinesis begins upon anaphase onset. An early step involves local activation of the small GTPase RhoA, which triggers assembly of an actomyosin-based contractile ring at the equatorial cortex. Here, we delineated the contributions of PLK1 and Aurora B to RhoA activation and cytokinesis initiation in human cells. Knock-down of PRC1, which disrupts the spindle midzone, revealed the existence of two pathways that can initiate cleavage furrow ingression. One pathway depends on a well-organized spindle midzone and PLK1, while the other depends on Aurora B activity and centralspindlin at the equatorial cortex and can operate independently of PLK1. We further show that PLK1 inhibition sequesters centralspindlin onto the spindle midzone, making it unavailable for Aurora B at the equatorial cortex. We propose that PLK1 activity promotes the release of centralspindlin from the spindle midzone through inhibition of PRC1, allowing centralspindlin to function as a regulator of spindle midzone formation and as an activator of RhoA at the equatorial cortex.

Introduction

Cytokinesis drives the physical separation of daughter cells at the end of mitosis. Failure to complete cytokinesis gives rise to tetraploid cells with supernumerary centrosomes. Depending on the cell type and cellular context, cytokinesis failure can either result in a G1 arrest or allow cell cycle progression of the tetraploid cells into the next mitosis (Andreassen et al., 2001; Uetake and Sluder, 2004). These dividing tetraploid cells are at risk of becoming aneuploid, owing to, for example, the extra number of centrosomes that can cause the missegregation of chromosomes during mitosis (Ganem et al., 2009; Silkworth et al., 2009; Tanaka et al., 2015). Hence, proper execution and completion of cytokinesis is essential for genomic stability.

In animal cells, cytokinesis starts in anaphase with the formation of an actomyosin-based contractile ring at the equatorial cortex that drives ingression of the cleavage furrow. Before membrane furrowing, interpolar microtubules are bundled between the separating sister chromatids to form the spindle midzone (also referred to as central spindle). As the furrow ingresses, these microtubule bundles are compacted into a cytoplasmic bridge, with the midbody in its center. The midbody attaches the ingressed cell membrane to the intercellular bridge and promotes the final phase of cytokinesis, known as abscission (Steigemann and Gerlich, 2009; Hu et al., 2012b; Lekomtsev et al., 2012; D'Avino and Capalbo, 2016). Formation of the contractile ring requires activation of the small GTPase RhoA by the guanine nucleotide exchange factor (GEF), ECT2 (Basant and Glotzer, 2018). Active, GTP-bound RhoA activates components of the actomyosin-based ring, such as diaphanous-related formin that facilitates the assembly of actin filaments (Otomo et al., 2005; Piekny et al., 2005; Watanabe et al., 2008; Chen et al., 2017) and Rho-kinase (ROCK), which activates nonmuscle myosin II to power ring constriction (Amano et al., 1996; Kosako et al., 2000). Optogenetic manipulation of RhoA activity showed that local activation of RhoA on the cell membrane is sufficient to drive cleavage furrow initiation independent of cell cycle stage (Wagner and Glotzer, 2016). Hence, strict spatial and temporal regulation of RhoA activity is essential to coordinate the onset of cytokinesis with nuclear division.

Current models for local RhoA activation and cleavage furrow initiation describe at least two anaphase spindle-derived stimulatory signals: one originating from the spindle midzone and another derived from astral microtubules that end at the equatorial cortex (Mishima, 2016). Experiments in large echinoderm embryos suggest a stimulatory role of astral microtubules in the initiation of cleavage furrow ingression (Su et al., 2014; Mishima, 2016), while data in smaller (mostly mammalian) cells emphasized a role for the spindle midzone (Cao and Wang, 1996). The overlapping antiparallel microtubules of the

[1]Oncode Institute, University Medical Center Utrecht, Utrecht University, Utrecht, Netherlands; [2]Center for Molecular Medicine, University Medical Center Utrecht, Utrecht University, Utrecht, Netherlands; [3]Department of Molecular Genetics and Cell Biology, University of Chicago, Chicago, IL.

Correspondence to Susanne M.A. Lens: s.m.a.lens@umcutrecht.nl; A. Basant's present address is Cellular Signalling and Cytoskeletal Function Lab, The Francis Crick Institute, London, England, UK.

spindle midzone serve as a platform for the localization of a variety of proteins that promote RhoA activation and cleavage furrow ingression directly parallel to the microtubule overlap. In addition, astral microtubules convey inhibitory signals at cell poles (Werner et al., 2007; Wagner and Glotzer, 2016; Mangal et al., 2018).

Protein regulator of cytokinesis 1 (PRC1) is essential for the assembly of a fully functional spindle midzone (Mollinari et al., 2002, 2005; Zhu et al., 2006). PRC1 is a homodimeric microtubule-binding protein that is directly involved in bundling antiparallel microtubules (Li et al., 2018). Its microtubule-bundling activity is required for spindle midzone formation, thereby indirectly contributing to the recruitment of other spindle midzone–localized proteins, such as centralspindlin and the chromosomal passenger complex (Mollinari et al., 2005; Zhu et al., 2006). Furthermore, through interaction with the kinesin KIF4A and Polo-like kinase 1 (PLK1; Kurasawa et al., 2004; Zhu and Jiang, 2005), PRC1 also directly recruits regulatory proteins to the spindle midzone.

Centralspindlin is a heterotetramer consisting of two molecules of the kinesin-6 MKLP1 (KIF23) and two molecules of RACGAP1 (hsCyk4 and MgcRacGAP; Basant and Glotzer, 2018). Oligomerization of the complex is needed to bundle microtubules and organize the spindle midzone (Hutterer et al., 2009). In addition to microtubule bundling, centralspindlin promotes RhoA activation and cleavage furrow initiation (Somers and Saint, 2003; Yüce et al., 2005; Nishimura and Yonemura, 2006). This latter function of centralspindlin appears to rely on PLK1-dependent binding of RACGAP1 to ECT2 (Petronczki et al., 2007; Burkard et al., 2009; Wolfe et al., 2009). Mutation of PLK1 phosphorylation sites in the noncatalytic N terminus of RACGAP1 disrupts its interaction with the N-terminal BRCT domain in ECT2 and disturbs the initiation of cytokinesis (Burkard et al., 2009; Wolfe et al., 2009). In line, inhibition of PLK1 activity at anaphase onset prevents RhoA activation at the equatorial cortex and cleavage furrow ingression (Brennan et al., 2007; Petronczki et al., 2007). Because inhibition of PLK1 activity or expression of a RACGAP1 PLK1-phosphorylation site mutant disrupt the spindle midzone localization of ECT2, it was proposed that the spindle midzone localization of ECT2 is a determining factor for the spatial activation of RhoA at the equatorial cortex (Burkard et al., 2009; Wolfe et al., 2009).

The chromosomal passenger complex, consisting of inner centromere protein (INCENP), Survivin, Borealin, and Aurora B kinase, relocates from chromosomes to the spindle midzone and equatorial cortex at anaphase onset in an MKLP2 (KIF20A)-dependent manner (Gruneberg et al., 2004; Hümmer and Mayer, 2009; Kitagawa et al., 2013, 2014). One of the spindle midzone targets of Aurora B is the centralspindlin subunit MKLP1 (Guse et al., 2005; Neef et al., 2006). Phosphorylation of S708 of MKLP1 disrupts the interaction between MKLP1 and 14-3-3 proteins, permitting centralspindlin oligomerization (Guse et al., 2005; Douglas et al., 2010; Basant et al., 2015). In *Caenorhabditis elegans* embryos, Aurora B–induced oligomerization of centralspindlin promotes RhoA activation and cleavage furrow ingression, and Aurora B activity is largely dispensable when centralspindlin constitutively oligomerizes (Basant et al., 2015). However, in mammalian cells, inhibition of Aurora B kinase activity at anaphase onset does not prevent initiation of cytokinesis, though it does prevent completion of cytokinesis (Guse et al., 2005; Ahonen et al., 2009; Steigemann and Gerlich, 2009). This suggests that RhoA activation can occur in the absence of Aurora B activity in mammalian cells and that, in these cells, Aurora B activity appears to be more relevant at later stages of cytokinesis most likely by promoting the formation of the spindle midzone and midbody (D'Avino and Capalbo, 2016).

While the spindle midzone is considered to provide important cues for RhoA activation at the equatorial cortex in mammalian cells (Yüce et al., 2005; Nishimura and Yonemura, 2006; Petronczki et al., 2007; Burkard et al., 2009; Wolfe et al., 2009), knock-down of PRC1, which clearly disrupts the spindle midzone, does not impair RhoA activation and cleavage furrow ingression (Jiang et al., 1998; Mollinari et al., 2005; Zhu and Jiang, 2005; Zhu et al., 2006). This implies that spindle midzone–independent cues can also locally activate RhoA in small, mammalian cells. Here, we demonstrate that in the absence of PRC1, RhoA is activated at the equatorial cortex, at least in part, through centralspindlin oligomerization induced by cortical Aurora B activity. Remarkably, we find that in PRC1-deficient cells, cytokinesis initiation can occur in the absence of PLK1 activity. This alternative PLK1-independent route to RhoA activation has been overlooked because of an unrecognized inhibitory effect of PLK1 on PRC1 in anaphase. Specifically, we propose that PLK1 activity limits PRC1-dependent hyperbundling of spindle midzone microtubules and reduces centralspindlin sequestration at the spindle midzone, making it available for Aurora B to activate RhoA at the equatorial cortex.

Results

Disruption of the spindle midzone allows PLK1-independent RhoA activation and furrow ingression

In human cells lacking PRC1, cleavage furrow ingression takes place despite the absence of a well-organized spindle midzone that concentrates cytokinetic regulators (Mollinari et al., 2005; Zhu et al., 2006). This suggests the existence of spindle midzone–independent cues in human cells that contribute to the local concentration of active RhoA. To delineate this spindle midzone–independent pathway, we analyzed the contribution of key cytokinesis regulators to cytokinesis initiation in a PRC1 knock-down background. We first confirmed that after PRC1 knock-down the spindle midzone was severely disrupted, as shown by the disorganized appearance of midzone microtubules (Fig. 1, A and B). In addition, live cell imaging of anaphase cells depleted of PRC1 revealed that most cells exhibit full-cleavage furrow ingression followed by cleavage furrow regression (Fig. 1, C and D). The frequency and extent of furrow ingression was assessed, and a distinction was made between no furrow ingression and minimal furrow ingression (Fig. 1 D and Fig. S1 A).

Because PLK1 is a critical regulator of RhoA activation and cleavage furrow ingression (Petronczki et al., 2007; Burkard et al., 2009), we tested its involvement in spindle midzone–independent

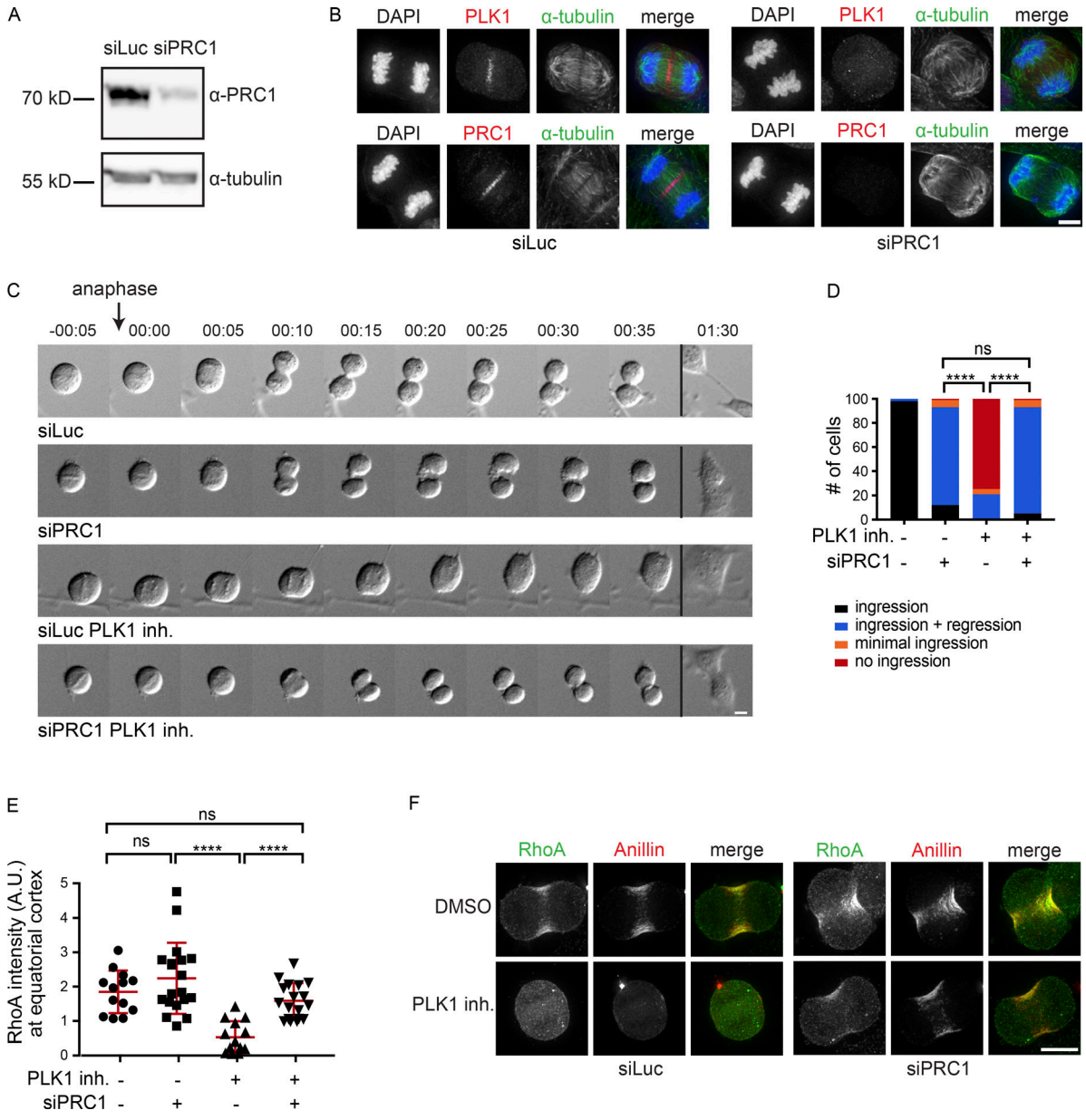

Figure 1. **PRC1 depletion reveals PLK1-independent RhoA activation and furrow ingression. (A)** Western blot of HeLa cells transfected with control siRNA (siLuc) or siRNA specific for PRC1. The Western blot was probed with an anti-PRC1 antibody. α-Tubulin is shown as loading control. **(B)** IF for PLK1, PRC1, and α-tubulin of HeLa cells transfected with siLuc or siPRC1. DNA was visualized using DAPI. **(C)** DIC stills of a live cell imaging experiment of HeLa cells transfected with either siLuc or siPRC1 with (PLK1 inh.) or without addition of BI2536 (100 nM) before anaphase onset. Time point 00:00 (hours:minutes) refers to the first frame where we observed separating sisters. Stills of more time frames are shown in Fig. S1 B. **(D)** Percentage of cells showing either complete furrow ingression, full-furrow ingression followed by furrow regression, visible but minimal furrow ingression, or no furrow ingression (n = 100 cells imaged per condition). ****, $P < 0.0001$; χ^2 test for comparison of the indicated conditions; ns, not significant. One representative experiment out of two is shown. **(E)** Quantification of fluorescence intensity levels of RhoA at the equatorial cortex in anaphase as shown in F. Each dot represents an individual cell. Error bars depict the SD of the mean. ****, $P < 0.0001$; Student's t test for comparison of the indicated conditions; ns, not significant. **(F)** IF for RhoA and Anillin of HeLa cells in anaphase transfected with the indicated siRNAs and treated with or without BI2536 (100 nM). Bars: 5 µm (B); 10 µm (C and F).

cytokinesis initiation. PLK1 activity was inhibited in metaphase, before anaphase onset, by addition of the small molecule inhibitor BI2536 (Steegmaier et al., 2007). Remarkably, while PLK1 inhibition alone completely prevented furrow ingression in ∼80% of control-transfected cells, PLK1 inhibition allowed full-furrow ingression in PRC1 knock-down cells (Fig. 1, C and D; and Fig. S1 B), after a ±5-min delay in the onset of furrow ingression (Fig. S1 C). PRC1 depletion restored RhoA and Anillin localization to the equatorial zone in PLK1-inhibited cells (Fig. 1, E and F). Thus, although PLK1 activity is critical for RhoA activation and initiation of cytokinesis in cells containing PRC1, it is dispensable when PRC1 is absent and the spindle midzone is disrupted. This suggests that PRC1 can function both as an activator and as an inhibitor of RhoA activation.

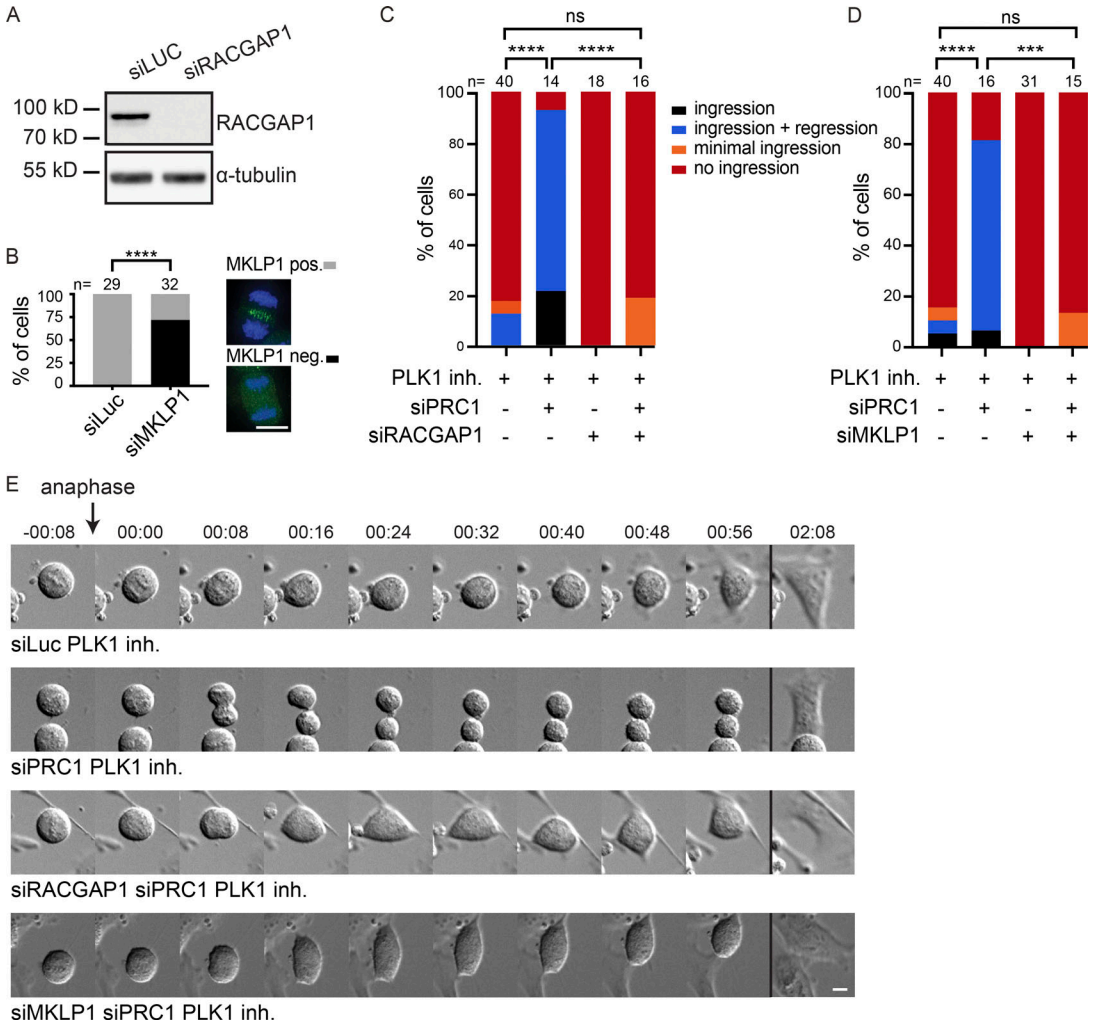

Figure 2. **PLK1-independent furrow ingression requires centralspindlin. (A)** Western blot of samples derived from HeLa cells transfected with either siLuc or siRACGAP1. The Western blot was probed with an anti-RACGAP1 antibody. α-Tubulin is shown as loading control. **(B)** HeLa cells were transfected with siLuc or siMKLP1 and processed for IF (right). The percentage of cells with detectable MKLP1 in anaphase was scored and used as a measure for knock-down efficiency (left). The number of cells that were scored per condition is indicated (n). One representative experiment out of two is shown. ****, $P < 0.0001$; χ^2 test for comparison of the indicated conditions. **(C and D)** HeLa cells transfected with the indicated siRNAs were imaged live. PLK1 was inhibited by addition of BI2536 (100 nM) before anaphase onset (PLK1 inh.). PLK1 was inhibited by addition of BI2536 (100 nM) before anaphase onset. The number of cells showing complete furrow ingression, full-furrow ingression followed by furrow regression, visible but minimal furrow ingression, or no furrow ingression was scored. The number of cells analyzed per condition is indicated (n). One representative experiment out of two is shown. ****, $P < 0.0001$; ***, $P < 0.001$; χ^2 test for comparison of the indicated conditions; ns, not significant. **(E)** DIC stills of HeLa cells transfected with the indicated siRNAs with or without addition of BI2536 (100 nM) before anaphase onset. Bars: 10 µm. Stills of more time frames are shown in Fig. S1 D.

PLK1-independent furrow ingression relies on the centralspindlin complex

The centralspindlin complex is an important target of PLK1 and involved in the activation of the RhoA GEF, ECT2 (Brennan et al., 2007; Santamaria et al., 2007; Burkard et al., 2009; Wolfe et al., 2009). We therefore tested whether centralspindlin is required for furrow ingression in cells depleted of PRC1 and treated with an inhibitor of PLK1 by depleting the two components of centralspindlin, RACGAP1 and MKLP1. Following RACGAP1 knock-down, the protein was indeed no longer detectable on Western blot (Fig. 2 A). MKLP1 knock-down was confirmed by immunofluorescence (IF), as the antibody failed to detect the protein on Western blot. The frequency of cells with undetectable MKLP1 localization in the anaphase midzone was used as a proxy for knock-down efficiency (Fig. 2 B). We combined PLK1 inhibition with knock-down of either PRC1, RACGAP1, or MKLP1, or with codepletion of PRC1 and RACGAP1, or of PRC1 and MKLP1 (Fig. 2, C–E; and Fig. S1 D). ∼80% of the siPRC1-transfected cells initiated cytokinesis when PLK1 was inhibited (Fig. 1 D and Fig. 2, C and D). However, cytokinesis initiation was almost completely blocked when RACGAP1 or MKLP1 was also depleted (Fig. 2, C–E; and Fig. S1 D). This demonstrates that while spindle midzone–independent furrow ingression does not require PLK1 activity, it does require centralspindlin. In *C. elegans* embryos, disruption of the spindle midzone by SPD-1 (the *C. elegans* orthologue of PRC1) depletion does not block furrowing (Verbrugghe and White, 2004; Lee et al., 2015). However, these earlier experiments were performed in the presence of NOP-1,

a nematode-specific ECT2 activator (Tse et al., 2011). Therefore, we tested whether RhoA activation and furrowing can occur in embryos deficient in both SPD-1 and NOP-1. All such embryos initiated furrow formation, though ∼50% of embryos did not complete furrow ingression. Furrow ingression was slower in the embryos depleted of SPD-1, but furrow initiation occurred more quickly following anaphase onset (Fig. S2 A). The more rapid initiation of furrowing may be a consequence of the more rapid and extensive spindle elongation (Fig. S2 B). In five out of eight embryos, RACGAP1 (CYK-4) was readily detected on the membrane during furrowing (Fig. S2 C). These results indicate conservation of a spindle midzone–independent and centralspindlin-dependent pathway for RhoA activation.

Aurora B activity at the equatorial cortex is required for spindle midzone–independent furrow ingression

By depleting PRC1, we uncovered a PLK1-independent but centralspindlin-dependent pathway for localized RhoA activation and furrow ingression. We hypothesized that another kinase might regulate centralspindlin-dependent RhoA activation and considered Aurora B kinase a likely candidate. Aurora B is located at the equatorial cortex in anaphase, and this localization becomes even more apparent after PRC1 depletion (Fig. 3 A; Earnshaw and Cooke, 1991; Murata-Hori and Wang, 2002; Mollinari et al., 2005). In both wild-type and PRC1-deficient cells, MKLP2 is required to relocalize the kinase from the chromosomes to the equatorial cortex (Fig. S3, A and B; Gruneberg et al., 2004; Hümmer and Mayer, 2009; Kitagawa et al., 2013). Moreover, we confirmed that this cortical localization of Aurora B was largely dependent on nonspindle midzone microtubules, because a concentration of nocodazole (83 nM) that did not depolymerize the stable spindle midzone microtubules, but removed microtubules outside the spindle midzone, reduced the localization of Aurora B at the equatorial cortex (Fig. 3 B and Fig. S3 C; O'Connell and Wang, 2000; Murata-Hori and Wang, 2002; Théry et al., 2005; Tame et al., 2014; Mishima, 2016). We next assessed the catalytic activity of this cortical pool of Aurora B. We fused a Förster resonance energy transfer (FRET)–based Aurora B phosphorylation sensor to the C-terminal (aa 243–505) Tubby domain of mouse Tubby protein, which binds phosphatidylinositol 4,5-biphosphate (PtdIns (4,5)P_2; Fig. 3 C; Santagata et al., 2001; Fuller et al., 2008; Szentpetery et al., 2009). The Tubby-FRET sensor was detected at the cell membrane before and during anaphase (Fig. 3 C). Although chromosome-bound Aurora B is active during (pro) metaphase (Fuller et al., 2008), we did not detect phosphorylation of the membrane-localized sensor in early mitosis (Fig. S3 D). Phosphorylation of the membrane-localized sensor becomes detectable at anaphase onset, before visible membrane ingression, and was most prominent at the equatorial cortex (Fig. 3, D–G). Depletion of MKLP2 or inhibition of Aurora B with ZM447439 before anaphase onset prevented the decrease in the YPet/mTFP1 emission ratio (Fig. S3, D–F).

Thus, an active pool of Aurora B kinase resides at the equatorial cortex at anaphase onset. To test the function of this pool of Aurora B, we inhibited Aurora B in both PRC1-proficient and PRC1-deficient cells. Inhibition of Aurora B activity in the presence of PRC1 did not prevent RhoA localization and Anillin accumulation at the equatorial cortex and did not block cleavage furrow ingression (Fig. 4, A–D; and Videos 1 and 2). In line with previous studies, only the later stages of cytokinesis were impaired after Aurora B inhibition, as cleavage furrows eventually regressed (Fig. 4, A and B; and Videos 1 and 2; Guse et al., 2005; Ahonen et al., 2009; Steigemann and Gerlich, 2009). However, in the absence of PRC1, cleavage furrow ingression and RhoA localization was fully dependent on Aurora B activity (Fig. 4, A–D; and Videos 3 and 4). In addition, knock-down of MKLP2, which prevents the accumulation of Aurora B at the equatorial cortex (Fig. S3 A), also impaired furrow ingression in PRC1-depleted cells (Fig. S3 B). This suggests a pivotal role for localized Aurora B in stimulating RhoA activity at the equatorial cortex when the spindle midzone is disrupted (Fig. 4, A–D). Of note, knock-down of PRC1 did not enhance Aurora B activity at the equatorial cortex (Fig. S3 G). This suggests that in the absence of PRC1, the spindle midzone–associated pool of Aurora B does not relocalize to the equatorial cortex to result in increased kinase activity. Thus, Aurora B activity is not critical for cytokinesis initiation in PRC1-proficient cells, but becomes essential for cleavage furrow ingression, after PRC1 depletion, when the spindle midzone is disrupted.

Aurora B–dependent centralspindlin localization and oligomerization contributes to spindle midzone–independent furrow ingression

MKLP1 is an established substrate of Aurora B (Guse et al., 2005), and phosphorylation of S708 in MKLP1 by Aurora B disrupts the binding of 14-3-3 proteins to MKLP1 (Douglas et al., 2010). Dissociation of 14-3-3 from MKLP1 promotes centralspindlin oligomerization, which supports spindle midzone formation in human cells (Hutterer et al., 2009) and cortical contractility in *C. elegans* embryos (Fig. 5 A; Basant et al., 2015). To test whether Aurora B–mediated centralspindlin oligomerization was responsible for spindle midzone–independent cytokinesis initiation in human cells, we generated a cell line stably expressing a phosphomimetic MKLP1-S708E variant (Fig. 5, B–D; and Fig. S4, A and B). Both GFP::MKLP1 and GFP::MKLP1 S708E localized to the midzone in anaphase and were capable of restoring RACGAP1 localization in a MKLP1 knock-down add-back experiment (Fig. S4 B). In otherwise wild-type cells, MKLP1 knock-down causes furrow regression after initial ingression, similar to what has been reported by others (Fig. 5 B; Yüce et al., 2005; Zhao and Fang, 2005; Kamijo et al., 2006; Nishimura and Yonemura, 2006; Nguyen et al., 2014). Expression of siRNA-resistant GFP::MKLP1 or GFP::MKLP1-S708E prevented furrow regression in the vast majority of the cells (Fig. 5 B), confirming the functionality of the siRNA-resistant, GFP-tagged MKLP1 proteins. Importantly, MKLP1-S708E rescued the initiation of cleavage furrow ingression in a fraction of cells double-depleted of PRC1 and MKLP1 and treated with the inhibitor of Aurora B (Fig. 5 B). Collectively, this suggests that in PRC1 knock-down cells, Aurora B induces local clustering of centralspindlin that contributes to RhoA activation and implies that at least some centralspindlin resides at the equatorial cortex. To test the latter, we performed live cell imaging experiments

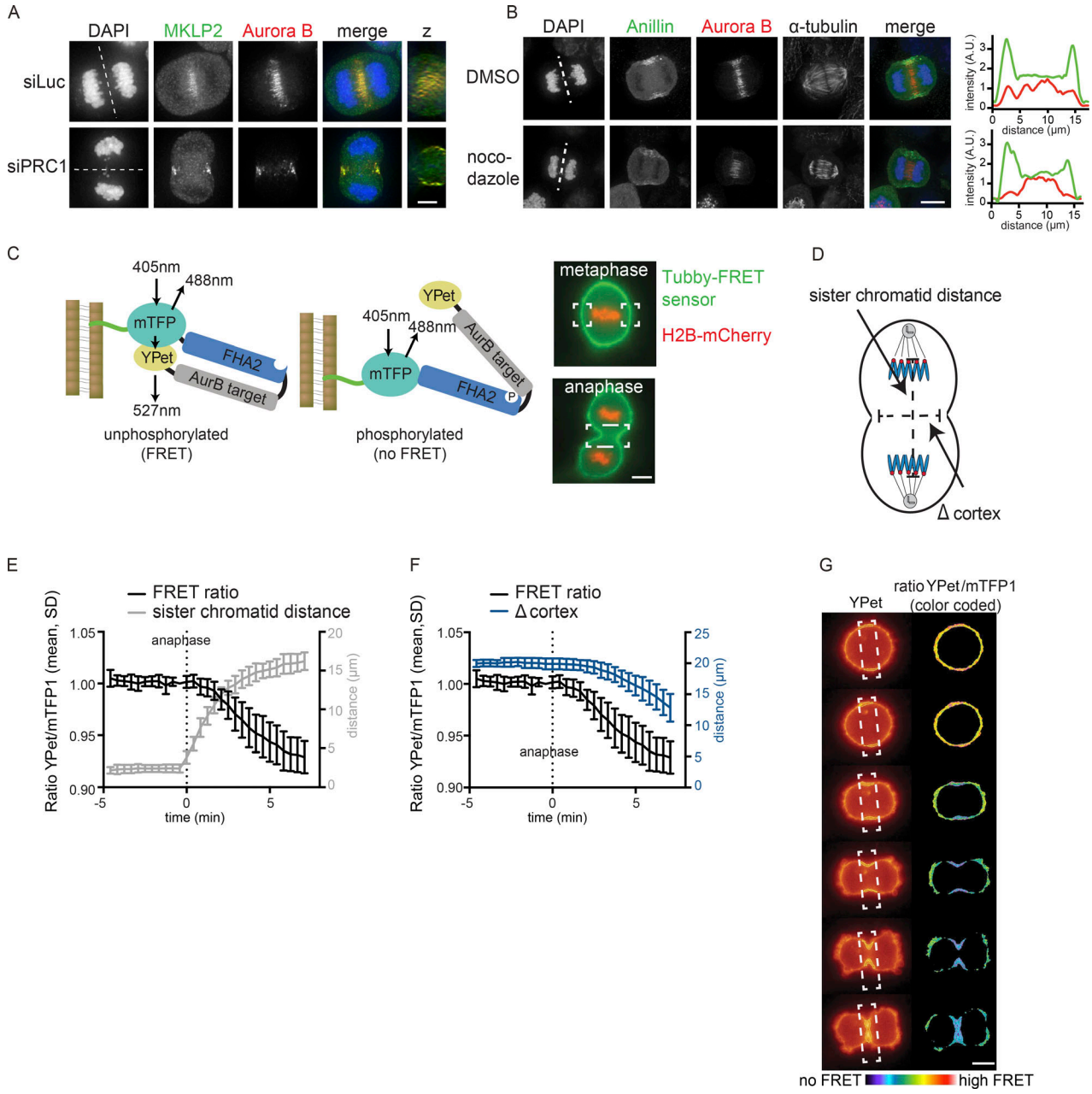

Figure 3. **Aurora B localization and activity at the equatorial cortex. (A)** IF for MKLP2 and Aurora B in HeLa cells transfected with siLuc or siPRC1. Dotted line indicates z plane for z-axis view. **(B)** IF for Anillin and Aurora B in anaphase cells treated with 83 nM nocodazole to depolymerize microtubules that are not part of the spindle midzone. Dotted line indicates z plane for line plot analysis of Anillin (green) and Aurora B (red) intensity (far right). **(C)** Left: Scheme of the FRET-based Aurora B biosensor fused to Tubby protein (green line). Right: HeLa Flp-In T-Rex cells stably expressing Tubby-Aurora B FRET sensor (green) and H2B-mCherry (red). White boxes indicate the areas where FRET was measured. **(D)** Measurement of distance between the separating sister chromatids and the width of the ingressing furrow (Δ cortex). **(E and F)** HeLa cells stably expressing the Tubby-Aurora B FRET sensor and H2B-mCherry were synchronized in G2 by treatment with the CDK1 inhibitor RO3306 and imaged live after release from the G2 block. The emission ratio at the equatorial cortex was calculated for each time point (interval, 25 s; mean ± SD of 10 cells) and plotted with the distance between the separating sister chromatids (E) or with the width of the ingressing furrow (F). **(G)** Color-coded images of the YPet/mTFP1 emission ratios. Bars: 5 µm (A and B); 10 µm (C and G).

with GFP::MKLP1 and RACGAP1::GFP in PRC1-depleted cells. After PRC1 knock-down, GFP::MKLP1 and RACGAP1::GFP no longer localized to microtubules in the midzone region (Fig. 5 C; Mollinari et al., 2005), but were detected at the equatorial cortex (Fig. 5 C). Of note, we failed to detect MKLP1 at the equatorial cortex and only infrequently detected RACGAP1 at this site when we performed IF on fixed cells (data not shown), implying that these proteins are weakly bound to the cortex and most likely were lost during fixation. Furthermore, GFP::MKLP1 was no longer detected at the equatorial cortex in PRC1-depleted cells when Aurora B kinase activity was inhibited, while GFP::MKLP1-S708E was detected (Fig. 5 D). Similarly, in 21 out of 32 cells analyzed, RACGAP1::GFP was also no longer detected at the equatorial cortex in PRC1-depleted cells when Aurora B kinase activity was

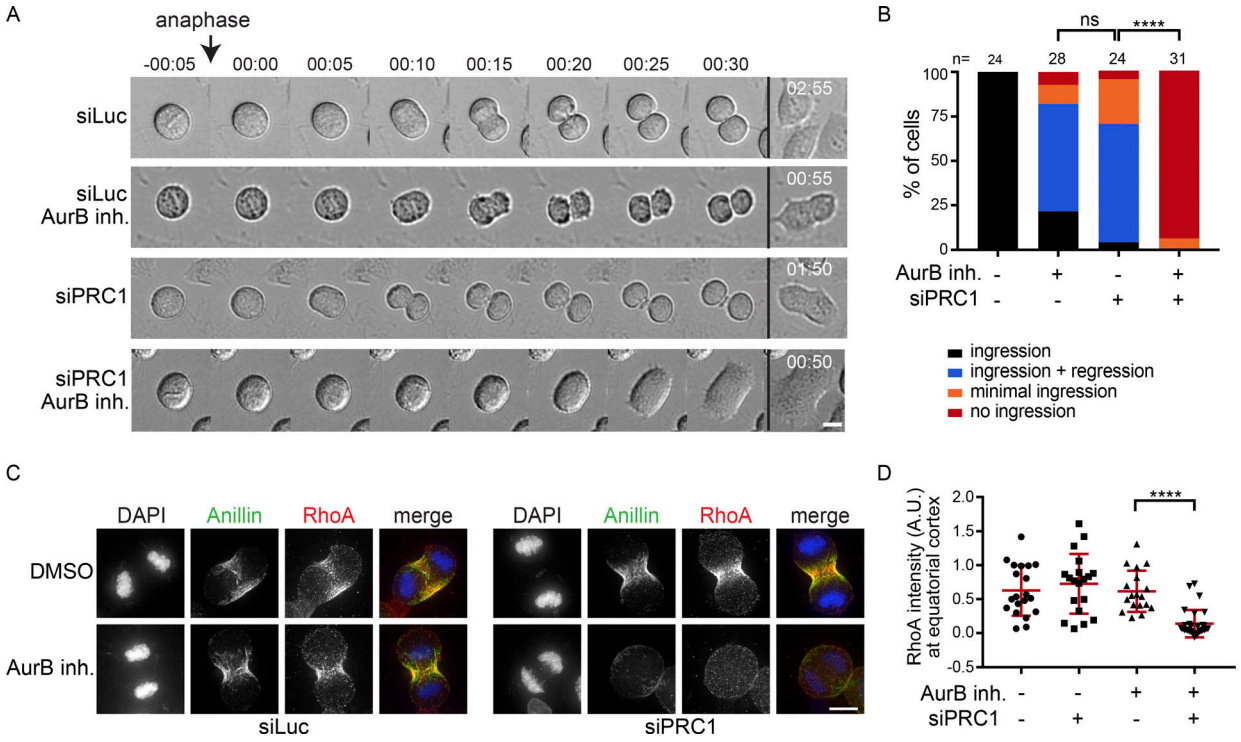

Figure 4. **Aurora B activity at the equatorial cortex is required for spindle midzone–independent furrow ingression. (A)** Representative brightfield stills of a live cell imaging experiment with HeLa cells transfected with the indicated siRNAs and treated with (AurB inh.) or without the Aurora B inhibitor ZM447439 (2 µM) before anaphase onset. **(B)** Cells were treated and imaged as in A, and the percentage of cells showing either stable furrow ingression, furrow ingression followed by furrow regression, minimal furrow ingression, or no furrow ingression was scored. The number of cells analyzed per condition is indicated (n). One representative experiment out of two is shown. ****, $P < 0.0001$; χ^2 test for comparison of the indicated conditions; ns, not significant. **(C)** IF for Anillin and RhoA. DNA was visualized using DAPI. **(D)** Quantification of the fluorescence intensity levels of RhoA at the equatorial cortex in anaphase. Each dot represents an individual cell. Error bars depict the SD of the mean. ****, $P < 0.0001$; Student's *t* test for comparison of the indicated conditions. Bars: 10 µm (A and C).

inhibited (Fig. S4 C). This implies that cortical Aurora B activity contributes to the recruitment or accumulation of centralspindlin to the equatorial cortex, most likely through phosphorylation of S708 in MKLP1.

In line with the findings in human cells, in *C. elegans* embryos, the homologue of RACGAP1 (CYK4) can be detected on the equatorial plasma membrane as the furrow ingresses (Fig. 5, E and F; and Video 5). Depletion of Aurora B (AIR-2) in these cells results in a measurable loss of membrane accumulation of centralspindlin (Fig. 5, E and F; and Video 6). Based on these collective findings, we propose that in human cells a small or a highly dynamic pool of centralspindlin at the equatorial cortex is sufficient to drive initiation of cytokinesis.

PLK1 suppresses PRC1 to limit sequestration of centralspindlin on the spindle midzone

Our findings suggest that RhoA activation at the equatorial cortex can occur by both PLK1-dependent and -independent cues, and that PLK1-independent RhoA activation requires Aurora B. If these cytokinesis initiation routes act strictly in parallel, inhibition of one pathway would still allow the other pathway to operate. This is indeed observed after Aurora B inhibition, but not after PLK1 inhibition. Why does furrow ingression fail when PLK1 is inhibited in PRC1-proficient cells, when, according to our model, Aurora B should suffice to activate RhoA? One explanation could be that PLK1 inhibits cortical Aurora B activity when PRC1 is present. To test this possibility, we used the membrane-localized FRET-based Aurora B biosensor and found that Aurora B was equally active at the equatorial cortex in PLK1-inhibited cells as in cells with active PLK1 in which the furrow ingressed (Fig. 6 A). We then asked whether PLK1 inhibition affects availability of Aurora B substrates at the cortex. PLK1 activity has been shown to limit the extent of PRC1-dependent microtubule bundling and centralspindlin recruitment to the mitotic spindle in metaphase (Hu et al., 2012b). This prompted us to investigate whether PLK1 also limits PRC1 activity at the spindle midzone in anaphase. Indeed, spindle midzone microtubules appeared more bundled in PLK1-inhibited anaphase cells, and this was diminished after PRC1 depletion (Fig. 6 B). Moreover, quantification of the levels of MKLP1, RACGAP1, and PRC1 at the spindle midzone revealed that the levels of these proteins increased when PLK1 is inhibited (Fig. 6, C and D; and Fig. S5, A and B). Moreover, PRC1 knockdown in PLK1-inhibited cells allowed localization of centralspindlin at the equatorial cortex (Fig. 6 C). Based on this, we hypothesized that PLK1 limits the extent of PRC1-mediated microtubule bunding and spindle midzone recruitment of centralspindlin in anaphase. As a corollary, we hypothesized that PRC1 promotes excessive recruitment of centralspindlin

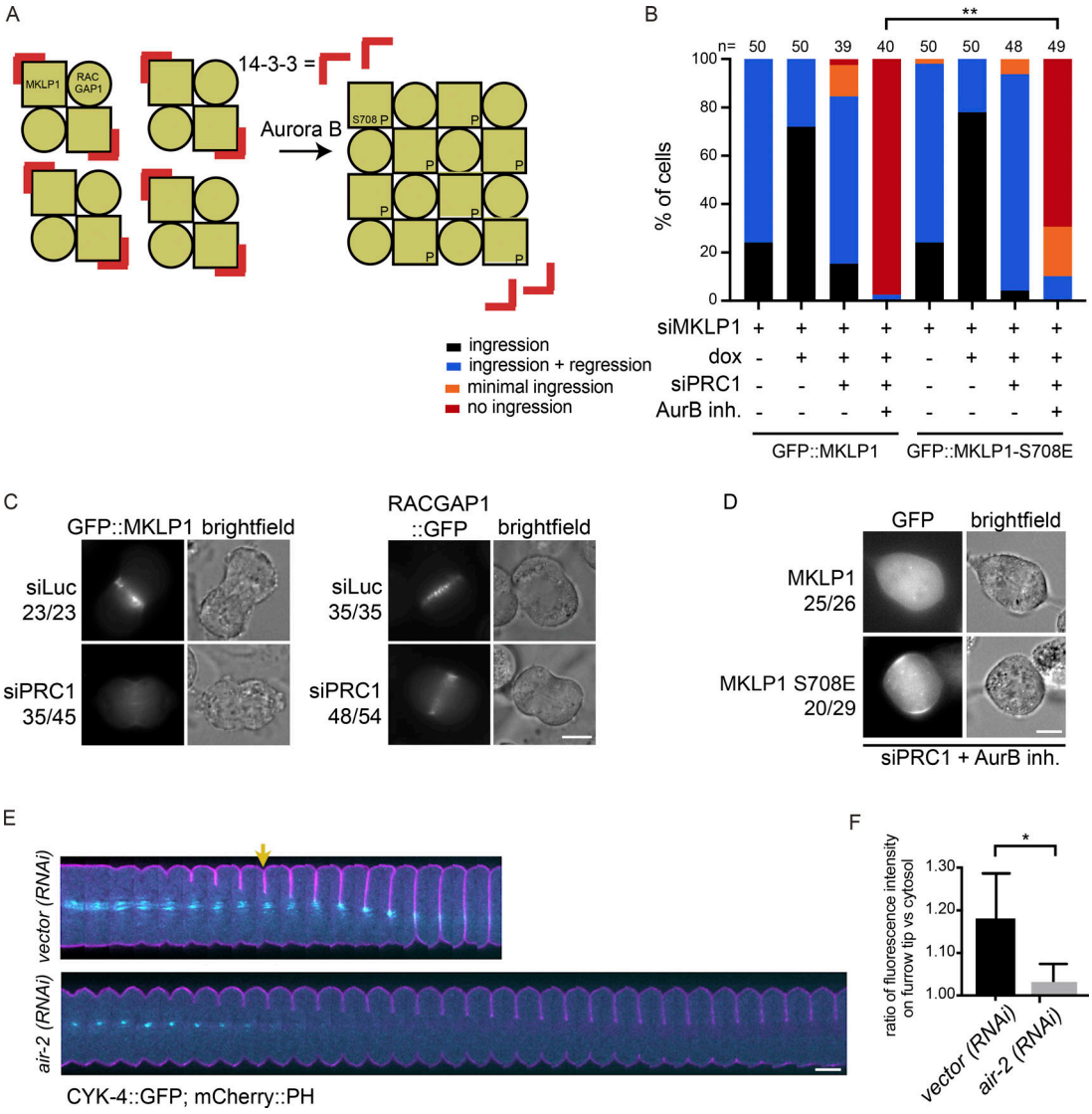

Figure 5. **Aurora B–dependent centralspindlin oligomerization contributes to spindle midzone–independent furrow ingression. (A)** Scheme explaining how oligomerization of centralspindlin is induced by Aurora B–dependent phosphorylation of MKLP1. **(B)** HeLa cell lines with stable inducible expression of GFP::MKLP1 and GFP::MKLP1-S708E were transfected with the indicated siRNAs, treated with or without ZM447439 before anaphase, and imaged live. The number of cells showing stable furrow regression, full-furrow regression followed by furrow regression, visible but minimal furrow ingression or no furrow ingression was scored. The number of cells analyzed per condition is indicated. One representative experiment out of three is shown. **, $P < 0.01$; χ^2 test for comparison of the indicated conditions. **(C)** Representative stills of HeLa cells in anaphase with stable inducible expression of GFP::MKLP1 and RACGAP1::GFP and transfected with the indicated siRNAs. Numbers indicate the number of times the depicted localization was observed/total number of cells that were imaged live. **(D)** Representative stills of HeLa cells in anaphase with stable inducible expression of GFP::MKLP1 and GFP::MKLP1-S708E and transfected with siPRC1 and treated with the Aurora B inhibitor ZM447439 (2 µM) before anaphase onset. **(E)** *C. elegans* embryos expressing a mCherry::PH membrane marker (pink) with a CYK-4::GFP transgene (cyan) were depleted of endogenous Aurora B (AIR-2) by RNAi. These embryos were filmed starting at metaphase in the first division cycle. Shown are montages of the equatorial region as the cell divides ($n \geq 5$). The arrow indicates the appearance of cortical CYK-4::GFP under wild-type conditions. **(F)** Embryos expressing CYK-4::GFP were scored for the extent of recruitment of the GFP marker to the ingressing furrow tip during anaphase, relative to a cytosolic background (see Materials and methods). Error bars represent ± SD; *, $P < 0.05$; Student's *t* test, $n \geq 5$. Bars: 10 µm (C–E).

to the spindle midzone when PLK1 is inhibited, thereby sequestering it away from the equatorial cortex. PRC1 depletion in PLK1-inhibited cells would release centralspindlin from the spindle midzone, allowing it to become activated by Aurora B at the equatorial cortex (Fig. 6 F). Based on this model, we reasoned that by overexpressing centralspindlin (via cooverexpression of GFP::MKLP1 and RACGAP1::GFP; Fig. S5 C), we could "saturate" the PRC1-dependent sequestering of centralspindlin to the spindle midzone after PLK1 inhibition and that some of the overexpressed centralspindlin would be available to mediate RhoA activation at the equatorial cortex and induce furrow ingression. Indeed, we found that centralspindlin overexpression promoted the initiation of cleavage furrow ingression in a substantial fraction of PLK1-inhibited, PRC1-proficient cells (Fig. 6 E).

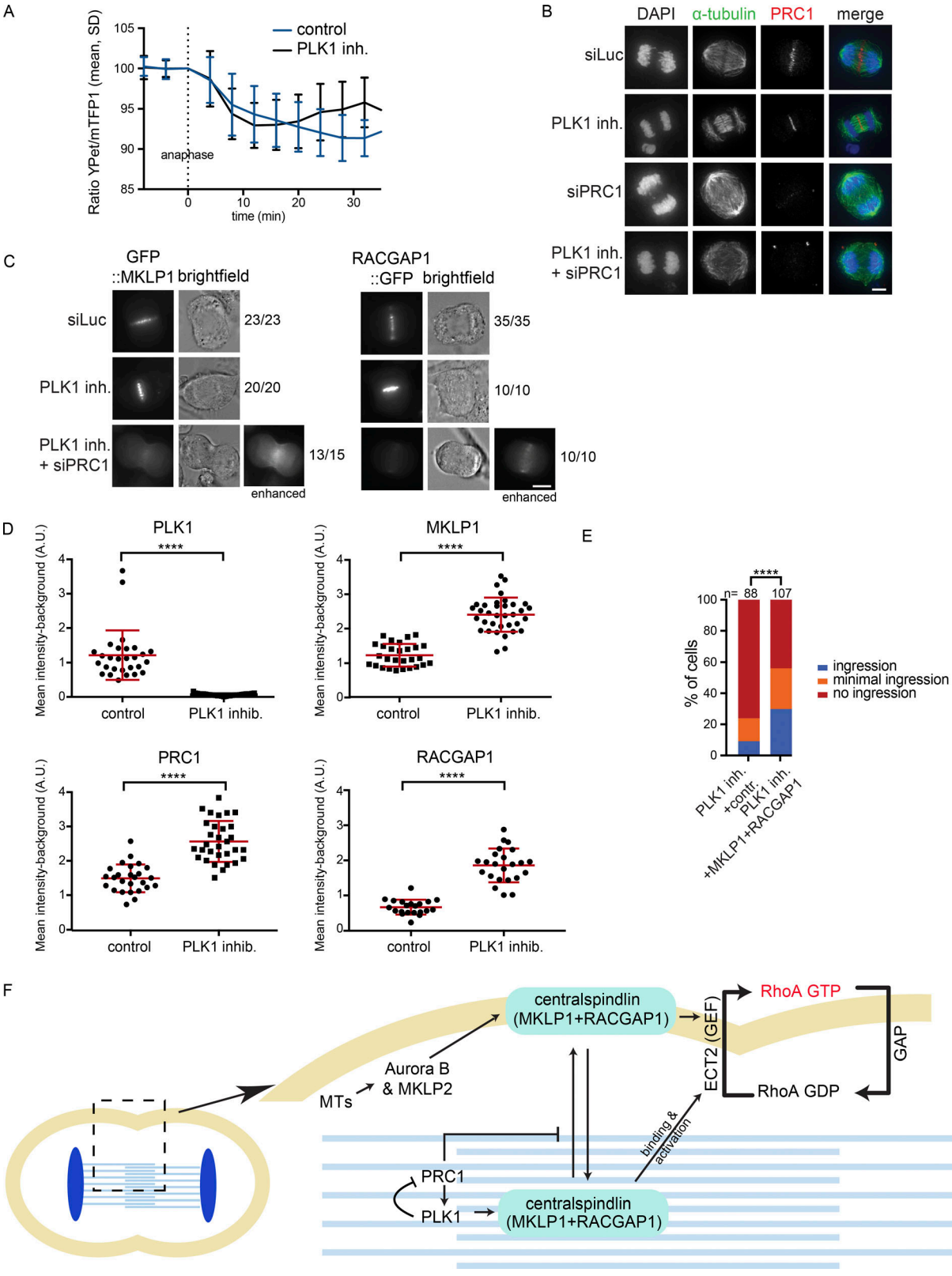

Figure 6. **PLK1 suppresses PRC1 to allow dynamic exchange of centralspindlin between the spindle midzone and cell cortex. (A)** HeLa cells stably expressing the Tubby-Aurora B FRET sensor and H2B-mCherry were synchronized in G2 using RO3306 and imaged live after release from the Cdk1 inhibitor. 35 min after release, BI2536 (100 nM) was added. The emission ratio at the equatorial cortex was calculated for each time point (interval, 5 min). Mean ± SD of 11 cells is shown. **(B)** IF for α-tubulin and PRC1 of HeLa cells in anaphase transfected with the indicated siRNAs and treated with or without BI2536. **(C)** Representative stills of HeLa cells in anaphase with stable inducible expression of GFP::MKLP1 and RACGAP1::GFP and transfected with the indicated siRNAs and treated with or without BI2536 (100 nM). Numbers indicate the number of times the depicted localization was observed/total number of cells that was

imaged live. See also Fig. S5 A. **(D)** Quantification of the IF intensity levels of PLK1, MKLP1, PRC1, and RACGAP1 at the spindle midzone in anaphase (see also Fig. S5 B). Each dot represents an individual cell. One representative experiment out of three is shown. Error bars depict SDs of the mean. ****, $P < 0.0001$ (Student's *t* test). **(E)** HeLa cells were infected with control GFP virus or with lentiviruses expressing GFP::MKLP1 and RACGAP1::GFP and were treated with BI2536 (100 nM) before anaphase onset and imaged live. The number of cells showing full-furrow ingression, visible but minimal furrow ingression, or no furrow ingression was scored. The number of cells analyzed per condition is indicated (n). ****, $P < 0.0001$; χ^2 test for comparison of the indicated conditions. **(F)** Model explaining how PLK1 and Aurora B activate centralspindlin and RhoA at the equatorial cortex. The phosphorylation of RACGAP1 by PLK1 promotes centralspindlin binding and activation of ECT2, while Aurora B most likely promotes ECT2 activation via oligomerization of centralspindlin after phosphorylation of MKLP1. PLK1 also exerts an inhibitory effect on PRC1 which promotes the release of a fraction of centralspindlin from the spindle midzone. MTs, microtubules. Bars: 5 µm (B); 10 µm (C).

Discussion

In this study we uncovered a PLK1-independent, Aurora B–dependent route to RhoA activation and cytokinesis initiation in human cells through knock-down of the microtubule-bundling protein PRC1. This PLK1-independent route to cytokinesis initiation has been missed, due to an unrecognized inhibitory effect of PLK1 on PRC1 in anaphase. We demonstrate that PLK1 constrains PRC1 in anaphase, which serves two purposes: first, it limits PRC1's microtubule-bundling activity; and second, it promotes the release of a (small) pool of centralspindlin from the spindle midzone. We argue this allows centralspindlin to function both as a regulator of spindle midzone formation and as an activator of RhoA at the equatorial cortex. How PLK1 constrains PRC1 remains to be fully determined. PRC1 is a direct substrate of PLK1, and its phosphorylation by PLK1 is needed to bind PLK1 and to localize the kinase on the spindle midzone (Neef et al., 2007; Hu et al., 2012a). This makes it inherently difficult to discriminate how PLK1 affects PRC1 function in anaphase, because mutation of the PLK1 phosphosites in PRC1 impairs PLK1 recruitment to the spindle midzone (Neef et al., 2007). PRC1 may directly sequester centralspindlin on the spindle midzone after PLK1 inhibition, as RACGAP1 can interact with PRC1 (Ban et al., 2004; Lee et al., 2015), or it may do so indirectly by creating hyperbundled microtubules in the midzone. Distinguishing these possibilities through structure-function analysis of PRC1 is also challenging because its overexpression results in precocious spindle binding during metaphase (Mollinari et al., 2005; Hu et al., 2012b; unpublished data).

An important implication from our work is that ECT2 and RhoA activation can occur in the absence of PLK1 activity. PLK1 was shown to activate the RhoA GEF, ECT2, through phosphorylation of RACGAP1, which promotes RACGAP1 binding to the autoinhibitory N terminus of ECT2. This relieves the intramolecular inhibition on the ECT2 GEF domain (Burkard et al., 2009; Wolfe et al., 2009; Zhang and Glotzer, 2015). The N terminus of RACGAP1 harbors four evolutionary conserved PLK1 phosphorylation sites, and mutating these sites to alanine (RACGAP1-4A) attenuates complex formation between centralspindlin and ECT2, fails to activate RhoA, and leads to loss of ECT2 from the spindle midzone (Burkard et al., 2009; Wolfe et al., 2009). These results point to a crucial role for PLK1 in activating ECT2 and RhoA. How can ECT2 and RhoA become activated in PRC1-depleted cells when PLK1 is inhibited? Our results are complementary to recent work that demonstrates that mutations in the N-terminal BRCT domains of ECT2 that strongly reduce its binding to RACGAP1 and its localization to the spindle midzone do not prevent equatorial RhoA activity and cleavage furrow ingression and supported cytokinesis (Kotýnková et al., 2016). Importantly, knock-down of RACGAP1 still impaired furrow ingression in cells reconstituted with the RACGAP1 binding–deficient ECT2 mutant (Kotýnková et al., 2016), as it does in PLK1-inhibited cells depleted of PRC1 (this study). Thus, RhoA activation during cytokinesis appears to be highly dependent on ECT2 activation by centralspindlin. Notably, the ECT2–RACGAP1 interaction is enhanced by, but does not require, RACGAP1 phosphorylation by PLK1 (Somers and Saint, 2003; Yüce et al., 2005). RACGAP1 contains a C-terminal GAP domain that also interacts with ECT2, which may contribute to formation and function of this complex (Zhang and Glotzer, 2015). This mode of ECT2 activation (and thereby RhoA activation) might require, or be strongly promoted by, localized centralspindlin oligomerization at the equatorial cortex, driven by Aurora B–dependent disengagement of 14-3-3 proteins from centralspindlin (Douglas et al., 2010; Basant et al., 2015).

This view is supported by optogenetic experiments with a C-terminally truncated ECT2 that only activates RhoA at the equator (Kotýnková et al., 2016), presumably due to the presence of centralspindlin at this site. Moreover, active Aurora B is present at the equatorial cortex in PRC1-depleted cells and may provide a local environment for centralspindlin oligomerization. Indeed, in *C. elegans*, centralspindlin oligomerization obviates the requirement for Aurora B activity (Basant et al., 2015). In cultured human cells, Aurora B activity is required for furrow ingression in PRC1-depleted cells and expression of MKLP1-S708E, mimicking Aurora B phosphorylation, partly restores ingression defects caused by Aurora B inhibition. This supports the idea that centralspindlin oligomerization can drive RhoA activation independent of PLK1. However, MKLP1-S708E, only rescues furrow ingression in small fraction of the PRC1-depleted and Aurora B–inhibited HeLa cells. This infers that Aurora B–dependent furrow ingression in PRC1-depleted cells is not solely explained by the phosphorylation of a single residue in a single Aurora B substrate (i.e., MKLP1-S708). In fact, Aurora B phosphorylates several other substrates during anaphase, such as RACGAP1, vimentin, SHCBP1 (SHC binding and spindle associated 1), and possibly myosin light chain and the myosin-binding subunit of myosin phosphatase, which all contribute to furrow ingression and cytokinesis in human cells (Goto et al., 2003; Yokoyama et al., 2005; Hengeveld et al., 2012; Asano et al., 2013).

One could argue that the main role of PLK1 in cytokinesis initiation is to limit PRC1 activity to make centralspindlin available for Aurora B–dependent activation at the equatorial cortex. However, in such a scenario, inhibition of Aurora B would always impair cytokinesis initiation, and this is not the

case: in PRC1-proficient cells, furrow ingression takes place when Aurora B is inhibited. This implies that PLK1-dependent RACGAP1 phosphorylation and activation of ECT2 at the spindle midzone, and Aurora B at the equatorial cortex, can in principle function as two separate pathways to centralspindlin and RhoA activation, and cytokinesis initiation. We propose that in wild-type cells, the "PLK1 brake" on PRC1 will also support the release of PLK1-phosphorylated centralspindlin bound to ECT2, from the spindle midzone, allowing it to reach and activate RhoA at the equatorial cortex. Together, the PLK1- and Aurora B–dependent pathways to centralspindlin and RhoA activation may confer robustness to and proper timing of the processs of cleavage furrow ingression in mammalian cells.

In cells expressing the ECT2 binding–deficient RACGAP-4A mutant, PLK1 is active and expected to act on PRC1, allowing the release of a fraction of centralspindlin from the spindle midzone that can then become activated at the equatorial cortex. In other words, the Aurora B–dependent route to furrow ingression should be operational. However, cleavage furrow ingression does not take place in the RACGAP1-4A–expressing cells (Wolfe et al., 2009). Interestingly, the RACGAP1-4A mutant appears more concentrated at the spindle midzone (Wolfe et al., 2009), similar to what is observed for endogenous RACGAP1 after PLK1 inhibition. This raises the question whether RACGAP1 phosphorylation by PLK1 might also promote the release of centralspindlin from the spindle midzone.

In conclusion, we provide evidence for the existence of two pathways resulting in centralspindlin and RhoA activation and cytokinesis initiation in human cells. One pathway depends on PLK1 and originates at the spindle midzone, and the other pathway depends on Aurora B activity at the equatorial cortex. We argue that this latter pathway has gone unnoticed due to an unrecognized inhibitory effect of PLK1 on PRC1 in anaphase. We propose that the PLK1-dependent "brake" on PRC1 is necessary to release a fraction of centralspindlin from the spindle midzone that can activate RhoA at the equatorial cortex. The finding that these two routes to centralspindlin and RhoA activation could operate independent from each other highlights the robustness and plasticity of centralspindlin-induced cleavage furrow formation.

Materials and methods

Cell culture

HeLa cells and HeLa Flp-In T-Rex cells were cultured in DMEM (Sigma-Aldrich) supplemented with 6% FCS (FBS; Sigma-Aldrich), 2 mM UltraGlutamine, and 100 U/ml penicillin and 100 µg/ml streptomycin (Lonza). Culture medium of HeLa Flp-In T-Rex cells and of all HeLa Flp-In T-Rex–derived cell lines (described below) was additionally supplemented with 4 µg/ml Blasticidin (PAA Laboratories). All cell lines were cultured at 37°C with 5% CO_2.

Plasmids

cDNA encoding the membrane-binding Tubby domain of mouse Tubby protein (aa 243–505; Szentpetery et al., 2009) was obtained by PCR from a mouse brain cDNA library and was subsequently cloned into a pcDNA3 vector containing a mTFP1 and YPet FRET-based sensor for Aurora B activity (Fuller et al., 2008; Wurzenberger et al., 2012). The CyPet donor of the original construct was replaced by mTFP1. Full-length, wild-type MKLP1 was amplified by PCR from a human thymus cDNA library and cloned into a pEGFP-C1 vector (Clontech) and subsequently cloned into a pcDNA5/FRT/TO vector (Invitrogen) in which the hygromycin B resistance cassette was replaced by a puromycin B resistance cassette (pcDNA5/FRT/TO-puro). Point mutations were introduced by site-directed mutagenesis. Full-length, wild-type RACGAP1::GFP (Wolfe et al., 2009) was cloned into a pcDNA5/FRT/TO-hygromycin B vector (Invitrogen). For lentiviral production, GFP::MKLP1 and RACGAP1::GFP were cloned in a pHAGE vector. As a control virus pHAGE-EFs-PCP-3×GFPnls (gift of T. Pederson [University of Massachusetts, Worcester, MA]; Addgene no. 75385; Ma et al., 2016) was used.

siRNA and plasmid transfection, viral production, and transduction

HeLa cells were transfected with siLuc (Luciferase GL2 duplex; 5′-CGUACGCGGAAUACUUCGAdTdT-3′; Dharmacon/D-001100-01-20), siPRC1 (ON-TARGETplus SMARTpool; 5′-ACAAGAACU GAGGUGGUA-3′, 5′-GCACGUAAGCUGAACACUA-3′, 5′-CCG GAAAGCGCUGCAAUUA-3′, and 5′-UAAAUCACCUUCGGGAAA U-3′; L-019491-00-0005), siMKLP2 (ON-TARGETplus SMART-pool; 5′-ACACAGGCCUUGAUGAUGA-3′, 5′-GGAACAUAGUCU UCAGGUA-3′, 5′-GGUUAAAGCUAAAUUACAG-3′, and 5′-GAA ACCAUUCCUUCGAAAU-3′; L-019491-00-0005), siMKLP1 (5′-CGACAUAACUUACGACAAAUU-3′), or siRACGAP1 (Thermo Fisher; HSS120934 Stealth siRNA; 5′-GCCAAGAACUGAGACAGA CAGUGUG-3′) with HiPerfect Transfection Reagent (no. 301705; Qiagen). The final concentration of siRNAs was 20 nM for siLuc, siPRC1, RACGAP1, and MKLP2. The final concentration of siRNAs for siMKLP1 was 40 nM. Cells were analyzed 48 h after siRNA transfection. A standard HiPerfect transfection protocol was used with a 3:1 ratio for siRNA:HiPerfect in Opti-MEM. Incubation of siRNA/HiPerfect mixture was done at 37°C for 20 min. Transient transfection of plasmids was performed with X-tremeGENE 9 DNA Transfection Reagent according the manufacturers protocol (Roche). To generate stable cell lines with doxycyclin-inducible expression of GFP::MKLP1, GFP::MKLP1-S708E and RACGAP1::GFP, HeLa Flp-In T-Rex cells were cotransfected with pOG44 (Invitrogen) and pcDNA5/FRT/TO-puromycin plasmids encoding the indicated proteins. After transfection cells were selected in medium supplemented with 2 µg/ml puromycin and 4 µg/ml blasticidin (Invitrogen). To generate HeLa Flp-In T-Rex cells stably expressing the Tubby-Aurora B FRET sensor, cells were transfected with a pcDNA3 plasmid encoding Tubby-Aurora B FRET sensor, and cells were selected and maintained in medium supplemented with 2 µg/ml puromycin (Sigma-Aldich) and 4 µg/ml blasticidin (Invitrogen). Finally, lentiviral particles were produced in HEK239T cells using third-generation packaging constructs (Dull et al., 1998). Supernatant containing viral particles was harvested 48 h after transfection and passed through a 45-µm filter. HeLa cells were transduced overnight in the presence of 4 µg/ml polybrene (Sigma-Aldrich).

Cell synchronization and inhibitor treatment

For live cell imaging and IF of anaphase cells, HeLa cells were plated in 2.5 mM thymidine (Sigma-Aldrich) for 24 h and released into 5 µM RO3306 (Calbiochem) for 16 h. Where indicated, doxycycline (1 µg/ml; Sigma-Aldrich) was added together with RO3306 to induce protein expression. Cells were released from the RO3306 block by washing three times with medium. HeLa cells were either filmed immediately after release from RO3306 or fixed 60 min after RO3306 release. Where indicated, BI2536 (100 nM final concentration; Selleck Chemicals) or ZM447439 (2 µM final concentration; Tocris Bioscience) was added 35 min after the RO3306 release. Alternatively, 83 nM DMSO or nocodazole (Sigma-Aldrich) was added 45 min after RO3306 release.

Western blot sample preparation, SDS-PAGE, and Western blotting

HeLa cells were synchronized in G1/S phase by a 24-h incubation with thymidine. After release from the thymidine block, cells were accumulated in mitosis by addition of S-Trityl-L-Cysteine (STLC, 20 µM; Tocris Bioscience) for 16 h. Mitotic enriched cells were collected and lysed in Laemmli buffer. Protein concentration was determined using a Lowry assay and protein samples were separated by SDS-PAGE and transferred to nitrocellulose membranes. Membranes were blocked in 4% milk in Tris-buffered Saline containing 0.5% Tween-20 (TBST) and subsequently incubated with the primary antibody for 2 h. Primary antibodies used were rabbit anti-PRC1 (Santa Cruz; sc-8356), mouse anti-α tubulin (Sigma-Aldrich; T5168), goat anti-RACGAP1 (Abcam; ab2270), and mouse anti-GFP (Roche; 11814460001). After washing the membranes with TBST, they were incubated with HRP-conjugated secondary antibodies (Bio-Rad). An enhance chemiluminescence detection kit (GE Healthcare) was used to visualize the protein–antibody complex.

IF microscopy

Cells were grown in 24-well plates containing 12-mm High Precision coverslips (Superior-Marienfeld GmbH & Co). Cells were fixed with 4% PFA in PBS for 7 min and permeabilized in either methanol (−20°C) or in 0.25% Triton X-100 in PBS for 5 min (RACGAP1). Cells were blocked in PBS containing 3% BSA and 0.1% Tween-20. Primary antibodies used were rabbit anti-KIF20A/MKLP2 (Bethyl [ITK]; A300-878A), rabbit anti-PRC1 (Santa Cruz; sc-8356), mouse anti–Aurora B (BD Transduction Laboratories; 611083), rabbit anti-Anillin (Piekny and Glotzer, 2008), mouse anti-RhoA (Santa Cruz; sc-418), rabbit anti-MKLP1 (Santa Cruz; sc-867), rabbit anti-PLK1 (Santa Cruz; sc-17783), rat anti–α-tubulin (Thermo Fisher; MA1-80017), goat anti-RACGAP1 (Abcam; ab2270). Secondary antibodies used were goat anti-mouse or goat anti-rabbit IgG–Alexa Fluor 488, goat anti-mouse or goat anti-rabbit IgG–Alexa Fluor 568, and goat anti-rat Alexa Fluor 647 (Invitrogen). In case of RACGAP1 staining, donkey anti-goat IgG–Alexa Fluor 568 was used in combination with chicken anti-mouse IgG–Alexa Fluor 488. For IF of RhoA, cells were fixed with 10% TCA in H_2O for 15 min on ice, washed three times with 30 mM glycine in PBS, and permeabilized for 5 min at room temperature in 0.25% Triton X-100 in PBS. Antibody dilutions and washes were done in 5% nonfat milk in PBS. DAPI was used for DNA staining and coverslips were mounted using ProLong Antifade (Molecular Probes). Images were taken with a Personal DeltaVision system (Applied Precision) equipped with a 100×/NA 1.40 UPLS Apo-UIS2 objective (Olympus) and a CoolSNAP HQ charge-coupled device (CCD) camera (Photometrics). Images were deconvolved in Softworx (Applied Precision). For each experiment, all images were acquired with identical illumination settings. Images are projections of deconvolved z stacks, unless stated otherwise. For visualization of the transversal plane, a 3D projection was made from a deconvolved z stack, and an image of the indicated viewpoint was used. Image analysis was performed with Fiji image processing software (ImageJ). To quantify and compare the mean fluorescence intensities (MFIs) in spindle midzone and equatorial cortex, a region of interest (ROI) of similar size for either the midzone or the equatorial cortex was used for each image to determine the MFIs in that area. Where indicated, using the same ROI, MFI in a random region of the cytoplasm was obtained as background measurement.

Live cell microscopy

Cells were seeded in µ-Slides (4 or 24 well; ibiTreat; Ibidi), except for the experiments presented in Fig. 1 D, Fig. 2 (C and D), Fig. 4 (A and B), Fig. 5 B, and Fig. S3 B, where cells were seeded in Corning Costar 24-well plates (Corning Inc.). Medium was changed to Leibovitz's medium (Sigma-Aldrich) supplemented with 10% FCS (FBS; Sigma-Aldrich), 2 mM UltraGlutamine, and 100 U/ml penicillin and 100 µg/ml streptomycin (Lonza) before live cell imaging. FRET sensor imaging was performed on an inverted Nikon Ti microscope with a Perfect Focus System. Imaging was performed at 37°C using a Microscope Cage Incubator (OkoLab), with a 63× oil NA 1.49 working distance 0.12 objective. The excitation filter, dichroic mirror, and emission filter for mTFP1 were 430/24×, Z465LP and 480/40 m. The excitation filter, dichroic mirror and emission filter for YFP were 500/20×, 89006bs, and 535/30m (Chroma). The emissions from both fluorophores were collected simultaneously from a single z plane using a TuCam beamsplitter and two Luca-EM-R-604 EMCCD cameras (Andor), controlled by company acquisition software (NIS Elements). Images were acquired using an Olympus IX-81 microscope with a 20× DIC UPLFLN NA 0.5 objective and a Hamamatsu ORCA-ER CCD camera and a 37°C heated chamber, controlled by Cell-M software. Note that in case of seeding in Corning Costar plates, we acquired brightfield images, while seeding in µ-Slides allowed us to acquire differential interference contrast (DIC) images. Image analysis was performed with Fiji image processing software (ImageJ). Exception: the scoring of phenotypes in Fig. 1 D was done using a 10× CPLFLN NA 0.3 objective to visualize more cells. The live cell images for GFP::MKLP1 and RACGAP1::GFP were acquired using an AxioImager Z1 (Zeiss) with a 63× long distance C-ApoChromat Korr water NA 1.15 objective with an Orca Flash V4.0 sCMOS camera (Hamamatsu) and a 37°C heated chamber, controlled by ZEN Pro 2.3 software. Single time point images were taken of cells in anaphase. Z stacks were made according to cell thickness with an optimal stepwidth of 0.27 µm. Image

analysis was performed with Fiji image processing software (ImageJ). To quantify and compare the MFIs in spindle midzone, a ROI of similar size for either the midzone or the equatorial cortex was used for each image to determine the MFIs in that area. Where indicated, using the same ROI, MFI in a random region of the cytoplasm was obtained (background).

FRET analysis

FRET sensor data analysis was done with a customized ImageJ FRET macro. Background emissions were measured by selecting a ROI adjacent to the cell cortex outside the cell. The background emissions were subtracted from both mTFP and YPet emissions and the YPet/mTFP ratio was calculated. Area selection was performed using thresholding and manual selection of the equatorial cell cortex.

C. elegans experiments

C. elegans strains were maintained on nematode growth medium plates using standard procedures. RNAi was administered by feeding nematodes with *Escherichia coli* expressing the appropriate double-stranded RNA (dsRNA; Timmons and Fire, 1998). *Spd-1* (RNAi) clone (WormBase ID: sjj_Y34D9A_151.d) and *air-2* (RNAi) clone (WormBase ID: sjj2_B0207.4) were obtained from a RNAi feeding library (Kamath et al., 2003). HT115 bacterial cultures were grown in Luria broth with 100 µg/ml ampicillin overnight at 37°C. Cultures (250 µl) were seeded on nematode growth medium plates containing 100 µg/ml ampicillin and 1 mM isopropyl β-d-1-thiogalactopyranoside and incubated at room temperature (~23°C) for 8 h. RNAi plasmids were obtained from a library produced by Kamath et al. (2003). L4 hermaphrodites were picked onto feeding plates at 25°C at least 24 h before dissection. To prepare one-cell embryos for imaging, gravid hermaphrodites were dissected into egg salt buffer on coverslips, mounted onto 2.5% agar pads, and sealed with vaseline. For confocal imaging, embryos were imaged with a 63×/1.4 NA oil-immersion lens on a Zeiss Axioimager M1 equipped with a Yokogawa CSU-X1 spinning-disk unit (Solamere) and illuminated with 50-mW, 488-nm and 50-mW, 561-nm lasers (Coherent). Images were captured on a Cascade 1K EMCCD camera controlled by MetaMorph (Molecular Devices). Image processing was performed with ImageJ. Time-lapse acquisitions were assembled into movies using Metamorph and ImageJ. MG731 (*nop-1(it142) III; xsSi43[cyk-4::gfp rRNAi, cb-unc-119(+)] II; mCherry::H2b; mCherry::PH)* and MG656 (*unc-119(ed3) III; ltIs44pAA173; [pie-1p-mCherry::PH(PLC1delta1) + unc-119(+)]; xsIs7[Myo2::GFP;CYK-4::GFP-Pie-1 3′UTR;UNC-119(wt)]*) embryos were filmed by time-lapse confocal and DIC microscopy. In the mCherry::PH or the DIC images, the tip of the furrow was defined by an ROI in ImageJ at different stages of ingression. The maximum intensity of CYK-4::GFP in the ROI was determined in the corresponding frames. Using the same ROI, a maximum intensity in a random region of the cytoplasm was obtained. The extent of recruitment to the furrow tip was calculated as (maximum furrow intensity/maximum cytosolic intensity − 1). These values were averaged across embryos of a given genotype.

Statistical analysis

Where indicated, the mean and SD are shown. Statistical significance was calculated with a χ^2 test or a Student's *t* test using Prism 7 software.

Online supplemental material

Fig. S1 shows an example of minimal furrow ingression, more time points for Fig. 1 C and Fig. 2 E, and quantifications of the extent of furrow ingression at different time points in PLK1-inhibited HeLa cells. Fig. S2 shows furrow ingression in *spd-1*–deficient *C. elegans* embryos. Fig. S3 demonstrates Aurora B localization and cytokinesis initiation in HeLa cells deficient in both PRC1 and MKLP2, quantifications of Aurora B levels corresponding to Fig. 3 B, and several controls for the Aurora B activity measurements with the Tubby-FRET sensor. Fig. S4 shows doxycycline-induced expression of GFP::MKLP1 proteins in HeLa cell lines and RACGAP::GFP localization in PRC1 knock-down cells, with or without active Aurora B. Fig. S5 shows localization of RACGAP1 and MKLP1 on the spindle midzone with or without active PLK1. In Video 1, HeLa cells transfected with siLuc were filmed (brightfield) starting at metaphase. In Video 2, HeLa cells transfected with siLuc and treated with the Aurora B inhibitor ZM447439 (2 µM) were filmed (brightfield). In Video 3, HeLa cells transfected with siPRC1 were filmed (brightfield) starting at prometaphase. In Video 4, HeLa cells transfected with siPRC1 and treated with the Aurora B inhibitor ZM447439 (2 µM) were filmed starting at metaphase (brightfield). In Video 5, *C. elegans* embryos expressing mCherry::PH membrane marker and CYK4::GFP were filmed starting at metaphase in the first division cycle. In Video 6, *C. elegans* embryos expressing mCherry::PH membrane marker and CYK4::GFP were depleted of endogenous Aurora B (AIR-2) by RNAi and filmed starting at metaphase in the first division cycle.

Acknowledgments

We thank Dr. D. Gerlich (Institute of Molecular Biotechnology, Vienna, Austria) for the plasmid containing the Aurora B FRET sensor.

This work is financially supported by the Netherlands Organization for Scientific Research (NWO-Vici 91812610 to S.M.A. Lens), by National Institutes of Health grant R01GM085087 (to M. Glotzer), and is part of the Oncode Institute which is partly financed by the Dutch Cancer Society.

The authors declare no competing financial interests.

Author contributions: I.E. Adriaans and S.M.A. Lens conceived the project. I.E. Adriaans, S.M.A. Lens, A. Basant, and M. Glotzer designed the experiments, and wrote the manuscript. I.E. Adriaans, B. Ponsioen, A. Basant, and M. Glotzer performed and analyzed the experiments.

Submitted: 8 May 2018
Revised: 26 December 2018
Accepted: 23 January 2019

References

Ahonen, L.J., A.M. Kukkonen, J. Pouwels, M.A. Bolton, C.D. Jingle, P.T. Stukenberg, and M.J. Kallio. 2009. Perturbation of Incenp function impedes anaphase chromatid movements and chromosomal passenger protein flux at centromeres. *Chromosoma.* 118:71–84. https://doi.org/10.1007/s00412-008-0178-0

Amano, M., M. Ito, K. Kimura, Y. Fukata, K. Chihara, T. Nakano, Y. Matsuura, and K. Kaibuchi. 1996. Phosphorylation and activation of myosin by Rho-associated kinase (Rho-kinase). *J. Biol. Chem.* 271:20246–20249. https://doi.org/10.1074/jbc.271.34.20246

Andreassen, P.R., O.D. Lohez, F.B. Lacroix, and R.L. Margolis. 2001. Tetraploid state induces p53-dependent arrest of nontransformed mammalian cells in G1. *Mol. Biol. Cell.* 12:1315–1328. https://doi.org/10.1091/mbc.12.5.1315

Asano, E., H. Hasegawa, T. Hyodo, S. Ito, M. Maeda, M. Takahashi, M. Hamaguchi, and T. Senga. 2013. The Aurora-B-mediated phosphorylation of SHCBP1 regulates cytokinetic furrow ingression. *J. Cell Sci.* 126:3263–3270. https://doi.org/10.1242/jcs.124875

Ban, R., Y. Irino, K. Fukami, and H. Tanaka. 2004. Human mitotic spindle-associated protein PRC1 inhibits MgcRacGAP activity toward Cdc42 during the metaphase. *J. Biol. Chem.* 279:16394–16402. https://doi.org/10.1074/jbc.M313257200

Basant, A., and M. Glotzer. 2018. Spatiotemporal Regulation of RhoA during Cytokinesis. *Curr. Biol.* 28:R570–R580. https://doi.org/10.1016/j.cub.2018.03.045

Basant, A., S. Lekomtsev, Y.C. Tse, D. Zhang, K.M. Longhini, M. Petronczki, and M. Glotzer. 2015. Aurora B kinase promotes cytokinesis by inducing centralspindlin oligomers that associate with the plasma membrane. *Dev. Cell.* 33:204–215. https://doi.org/10.1016/j.devcel.2015.03.015

Brennan, I.M., U. Peters, T.M. Kapoor, and A.F. Straight. 2007. Polo-like kinase controls vertebrate spindle elongation and cytokinesis. *PLoS One.* 2:e409. https://doi.org/10.1371/journal.pone.0000409

Burkard, M.E., J. Maciejowski, V. Rodriguez-Bravo, M. Repka, D.M. Lowery, K.R. Clauser, C. Zhang, K.M. Shokat, S.A. Carr, M.B. Yaffe, and P.V. Jallepalli. 2009. Plk1 self-organization and priming phosphorylation of HsCYK-4 at the spindle midzone regulate the onset of division in human cells. *PLoS Biol.* 7:e1000111. https://doi.org/10.1371/journal.pbio.1000111

Cao, L.G., and Y.L. Wang. 1996. Signals from the spindle midzone are required for the stimulation of cytokinesis in cultured epithelial cells. *Mol. Biol. Cell.* 7:225–232. https://doi.org/10.1091/mbc.7.2.225

Chen, A., P.D. Arora, C.A. McCulloch, and A. Wilde. 2017. Cytokinesis requires localized β-actin filament production by an actin isoform specific nucleator. *Nat. Commun.* 8:1530. https://doi.org/10.1038/s41467-017-01231-x

D'Avino, P.P., and L. Capalbo. 2016. Regulation of midbody formation and function by mitotic kinases. *Semin. Cell Dev. Biol.* 53:57–63. https://doi.org/10.1016/j.semcdb.2016.01.018

Douglas, M.E., T. Davies, N. Joseph, and M. Mishima. 2010. Aurora B and 14-3-3 coordinately regulate clustering of centralspindlin during cytokinesis. *Curr. Biol.* 20:927–933. https://doi.org/10.1016/j.cub.2010.03.055

Dull, T., R. Zufferey, M. Kelly, R.J. Mandel, M. Nguyen, D. Trono, and L. Naldini. 1998. A third-generation lentivirus vector with a conditional packaging system. *J. Virol.* 72:8463–8471.

Earnshaw, W.C., and C.A. Cooke. 1991. Analysis of the distribution of the INCENPs throughout mitosis reveals the existence of a pathway of structural changes in the chromosomes during metaphase and early events in cleavage furrow formation. *J. Cell Sci.* 98:443–461.

Fuller, B.G., M.A. Lampson, E.A. Foley, S. Rosasco-Nitcher, K.V. Le, P. Tobelmann, D.L. Brautigan, P.T. Stukenberg, and T.M. Kapoor. 2008. Midzone activation of aurora B in anaphase produces an intracellular phosphorylation gradient. *Nature.* 453:1132–1136. https://doi.org/10.1038/nature06923

Ganem, N.J., S.A. Godinho, and D. Pellman. 2009. A mechanism linking extra centrosomes to chromosomal instability. *Nature.* 460:278–282. https://doi.org/10.1038/nature08136

Goto, H., Y. Yasui, A. Kawajiri, E.A. Nigg, Y. Terada, M. Tatsuka, K. Nagata, and M. Inagaki. 2003. Aurora-B regulates the cleavage furrow-specific vimentin phosphorylation in the cytokinetic process. *J. Biol. Chem.* 278:8526–8530. https://doi.org/10.1074/jbc.M210892200

Gruneberg, U., R. Neef, R. Honda, E.A. Nigg, and F.A. Barr. 2004. Relocation of Aurora B from centromeres to the central spindle at the metaphase to anaphase transition requires MKlp2. *J. Cell Biol.* 166:167–172. https://doi.org/10.1083/jcb.200403084

Guse, A., M. Mishima, and M. Glotzer. 2005. Phosphorylation of ZEN-4/MKLP1 by aurora B regulates completion of cytokinesis. *Curr. Biol.* 15:778–786. https://doi.org/10.1016/j.cub.2005.03.041

Hengeveld, R.C.C., N.T. Hertz, M.J.M. Vromans, C. Zhang, A.L. Burlingame, K.M. Shokat, and S.M.A. Lens. 2012. Development of a chemical genetic approach for human aurora B kinase identifies novel substrates of the chromosomal passenger complex. *Mol. Cell. Proteomics.* 11:47–59. https://doi.org/10.1074/mcp.M111.013912

Hu, C.-K., M. Coughlin, and T.J. Mitchison. 2012a. Midbody assembly and its regulation during cytokinesis. *Mol. Biol. Cell.* 23:1024–1034. https://doi.org/10.1091/mbc.e11-08-0721

Hu, C.-K.K., N. Ozlü, M. Coughlin, J.J. Steen, and T.J. Mitchison. 2012b. Plk1 negatively regulates PRC1 to prevent premature midzone formation before cytokinesis. *Mol. Biol. Cell.* 23:2702–2711. https://doi.org/10.1091/mbc.e12-01-0058

Hümmer, S., and T.U. Mayer. 2009. Cdk1 negatively regulates midzone localization of the mitotic kinesin Mklp2 and the chromosomal passenger complex. *Curr. Biol.* 19:607–612. https://doi.org/10.1016/j.cub.2009.02.046

Hutterer, A., M. Glotzer, and M. Mishima. 2009. Clustering of centralspindlin is essential for its accumulation to the central spindle and the midbody. *Curr. Biol.* 19:2043–2049. https://doi.org/10.1016/j.cub.2009.10.050

Jiang, W., G. Jimenez, N.J. Wells, T.J. Hope, G.M. Wahl, T. Hunter, and R. Fukunaga. 1998. PRC1: a human mitotic spindle-associated CDK substrate protein required for cytokinesis. *Mol. Cell.* 2:877–885. https://doi.org/10.1016/S1097-2765(00)80302-0

Kamath, R.S., A.G. Fraser, Y. Dong, G. Poulin, R. Durbin, M. Gotta, A. Kanapin, N. Le Bot, S. Moreno, M. Sohrmann, et al. 2003. Systematic functional analysis of the Caenorhabditis elegans genome using RNAi. *Nature.* 421:231–237. https://doi.org/10.1038/nature01278

Kamijo, K., N. Ohara, M. Abe, T. Uchimura, H. Hosoya, J.-S. Lee, and T. Miki. 2006. Dissecting the role of Rho-mediated signaling in contractile ring formation. *Mol. Biol. Cell.* 17:43–55. https://doi.org/10.1091/mbc.e05-06-0569

Kitagawa, M., S.Y.S. Fung, N. Onishi, H. Saya, and S.H. Lee. 2013. Targeting Aurora B to the equatorial cortex by MKlp2 is required for cytokinesis. *PLoS One.* 8:e64826. https://doi.org/10.1371/journal.pone.0064826

Kitagawa, M., S.Y.S. Fung, U.F.S. Hameed, H. Goto, M. Inagaki, and S.H. Lee. 2014. Cdk1 coordinates timely activation of MKlp2 kinesin with relocation of the chromosome passenger complex for cytokinesis. *Cell Reports.* 7:166–179. https://doi.org/10.1016/j.celrep.2014.02.034

Kosako, H., T. Yoshida, F. Matsumura, T. Ishizaki, S. Narumiya, and M. Inagaki. 2000. Rho-kinase/ROCK is involved in cytokinesis through the phosphorylation of myosin light chain and not ezrin/radixin/moesin proteins at the cleavage furrow. *Oncogene.* 19:6059–6064. https://doi.org/10.1038/sj.onc.1203987

Kotýnková, K., K.-C. Su, S.C. West, and M. Petronczki. 2016. Plasma Membrane Association but Not Midzone Recruitment of RhoGEF ECT2 Is Essential for Cytokinesis. *Cell Reports.* 17:2672–2686. https://doi.org/10.1016/j.celrep.2016.11.029

Kurasawa, Y., W.C. Earnshaw, Y. Mochizuki, N. Dohmae, and K. Todokoro. 2004. Essential roles of KIF4 and its binding partner PRC1 in organized central spindle midzone formation. *EMBO J.* 23:3237–3248. https://doi.org/10.1038/sj.emboj.7600347

Lee, K.Y., B. Esmaeili, B. Zealley, and M. Mishima. 2015. Direct interaction between centralspindlin and PRC1 reinforces mechanical resilience of the central spindle. *Nat. Commun.* 6:7290. https://doi.org/10.1038/ncomms8290

Lekomtsev, S., K.C. Su, V.E. Pye, K. Blight, S. Sundaramoorthy, T. Takaki, L.M. Collinson, P. Cherepanov, N. Divecha, and M. Petronczki. 2012. Centralspindlin links the mitotic spindle to the plasma membrane during cytokinesis. *Nature.* 492:276–279. https://doi.org/10.1038/nature11773

Li, J., M. Dallmayer, T. Kirchner, J. Musa, and T.G.P. Grünewald. 2018. PRC1: Linking Cytokinesis, Chromosomal Instability, and Cancer Evolution. *Trends Cancer.* 4:59–73. https://doi.org/10.1016/j.trecan.2017.11.002

Ma, H., L.-C. Tu, A. Naseri, M. Huisman, S. Zhang, D. Grunwald, and T. Pederson. 2016. Multiplexed labeling of genomic loci with dCas9 and engineered sgRNAs using CRISPRainbow. *Nat. Biotechnol.* 34:528–530. https://doi.org/10.1038/nbt.3526

Mangal, S., J. Sacher, T. Kim, D.S. Osório, F. Motegi, A.X. Carvalho, K. Oegema, and E. Zanin. 2018. TPXL-1 activates Aurora A to clear contractile ring components from the polar cortex during cytokinesis. *J. Cell Biol.* 217:837–848. https://doi.org/10.1083/jcb.201706021

Mishima, M. 2016. Centralspindlin in Rappaport's cleavage signaling. *Semin. Cell Dev. Biol.* 53:45–56. https://doi.org/10.1016/j.semcdb.2016.03.006

Mollinari, C., J.-P. Kleman, W. Jiang, G. Schoehn, T. Hunter, and R.L. Margolis. 2002. PRC1 is a microtubule binding and bundling protein essential to maintain the mitotic spindle midzone. *J. Cell Biol.* 157:1175–1186. https://doi.org/10.1083/jcb.200111052

Mollinari, C., J.-P. Kleman, Y. Saoudi, S.A. Jablonski, J. Perard, T.J. Yen, and R. L. Margolis. 2005. Ablation of PRC1 by small interfering RNA demonstrates that cytokinetic abscission requires a central spindle bundle in mammalian cells, whereas completion of furrowing does not. *Mol. Biol. Cell.* 16:1043–1055. https://doi.org/10.1091/mbc.e04-04-0346

Murata-Hori, M., and Y.L. Wang. 2002. Both midzone and astral microtubules are involved in the delivery of cytokinesis signals: insights from the mobility of aurora B. *J. Cell Biol.* 159:45–53. https://doi.org/10.1083/jcb.200207014

Neef, R., U.R. Klein, R. Kopajtich, and F.A. Barr. 2006. Cooperation between mitotic kinesins controls the late stages of cytokinesis. *Curr. Biol.* 16: 301–307. https://doi.org/10.1016/j.cub.2005.12.030

Neef, R., U. Gruneberg, R. Kopajtich, X. Li, E.A. Nigg, H. Sillje, and F.A. Barr. 2007. Choice of Plk1 docking partners during mitosis and cytokinesis is controlled by the activation state of Cdk1. *Nat. Cell Biol.* 9:436–444. https://doi.org/10.1038/ncb1557

Nguyen, P.A., A.C. Groen, M. Loose, K. Ishihara, M. Wühr, C.M. Field, and T.J. Mitchison. 2014. Spatial organization of cytokinesis signaling reconstituted in a cell-free system. *Science.* 346:244–247. https://doi.org/10.1126/science.1256773

Nishimura, Y., and S. Yonemura. 2006. Centralspindlin regulates ECT2 and RhoA accumulation at the equatorial cortex during cytokinesis. *J. Cell Sci.* 119:104–114. https://doi.org/10.1242/jcs.02737

O'Connell, C.B., and Y.L. Wang. 2000. Mammalian spindle orientation and position respond to changes in cell shape in a dynein-dependent fashion. *Mol. Biol. Cell.* 11:1765–1774. https://doi.org/10.1091/mbc.11.5.1765

Otomo, T., C. Otomo, D.R. Tomchick, M. Machius, and M.K. Rosen. 2005. Structural basis of Rho GTPase-mediated activation of the formin mDia1. *Mol. Cell.* 18:273–281. https://doi.org/10.1016/j.molcel.2005.04.002

Petronczki, M., M. Glotzer, N. Kraut, and J.M. Peters. 2007. Polo-like kinase 1 triggers the initiation of cytokinesis in human cells by promoting recruitment of the RhoGEF Ect2 to the central spindle. *Dev. Cell.* 12: 713–725. https://doi.org/10.1016/j.devcel.2007.03.013

Piekny, A.J., and M. Glotzer. 2008. Anillin is a scaffold protein that links RhoA, actin, and myosin during cytokinesis. *Curr. Biol.* 18:30–36. https://doi.org/10.1016/j.cub.2007.11.068

Piekny, A., M. Werner, and M. Glotzer. 2005. Cytokinesis: welcome to the Rho zone. *Trends Cell Biol.* 15:651–658. https://doi.org/10.1016/j.tcb.2005.10.006

Santagata, S., T.J. Boggon, C.L. Baird, C.A. Gomez, J. Zhao, W.S. Shan, D.G. Myszka, and L. Shapiro. 2001. G-protein signaling through tubby proteins. *Science.* 292:2041–2050. https://doi.org/10.1126/science.1061233

Santamaria, A., R. Neef, U. Eberspächer, K. Eis, M. Husemann, D. Mumberg, S. Prechtl, V. Schulze, G. Siemeister, L. Wortmann, et al. 2007. Use of the novel Plk1 inhibitor ZK-thiazolidinone to elucidate functions of Plk1 in early and late stages of mitosis. *Mol. Biol. Cell.* 18:4024–4036. https://doi.org/10.1091/mbc.e07-05-0517

Silkworth, W.T., I.K. Nardi, L.M. Scholl, and D. Cimini. 2009. Multipolar spindle pole coalescence is a major source of kinetochore mis-attachment and chromosome mis-segregation in cancer cells. *PLoS One.* 4:e6564. https://doi.org/10.1371/journal.pone.0006564

Somers, W.G., and R. Saint. 2003. A RhoGEF and Rho family GTPase-activating protein complex links the contractile ring to cortical microtubules at the onset of cytokinesis. *Dev. Cell.* 4:29–39. https://doi.org/10.1016/S1534-5807(02)00402-1

Steegmaier, M., M. Hoffmann, A. Baum, P. Lénárt, M. Petronczki, M. Krssák, U. Gürtler, P. Garin-Chesa, S. Lieb, J. Quant, et al. 2007. BI 2536, a potent and selective inhibitor of polo-like kinase 1, inhibits tumor growth in vivo. *Curr. Biol.* 17:316–322. https://doi.org/10.1016/j.cub.2006.12.037

Steigemann, P., and D.W. Gerlich. 2009. Cytokinetic abscission: cellular dynamics at the midbody. *Trends Cell Biol.* 19:606–616. https://doi.org/10.1016/j.tcb.2009.07.008

Su, K.-C., W.M. Bement, M. Petronczki, and G. von Dassow. 2014. An astral simulacrum of the central spindle accounts for normal, spindle-less, and anucleate cytokinesis in echinoderm embryos. *Mol. Biol. Cell.* 25: 4049–4062. https://doi.org/10.1091/mbc.e14-04-0859

Szentpetery, Z., A. Balla, Y.J. Kim, M.A. Lemmon, and T. Balla. 2009. Live cell imaging with protein domains capable of recognizing phosphatidylinositol 4,5-bisphosphate; a comparative study. *BMC Cell Biol.* 10:67. https://doi.org/10.1186/1471-2121-10-67

Tame, M.A., J.A. Raaijmakers, B. van den Broek, A. Lindqvist, K. Jalink, and R. H. Medema. 2014. Astral microtubules control redistribution of dynein at the cell cortex to facilitate spindle positioning. *Cell Cycle.* 13:1162–1170. https://doi.org/10.4161/cc.28031

Tanaka, H., H. Goto, A. Inoko, H. Makihara, A. Enomoto, K. Horimoto, M. Matsuyama, K. Kurita, I. Izawa, and M. Inagaki. 2015. Cytokinetic failure-induced tetraploidy develops into aneuploidy, triggering skin aging in phosphovimentin-deficient mice. *J. Biol. Chem.* 290: 12984–12998. https://doi.org/10.1074/jbc.M114.633891

Théry, M., V. Racine, A. Pépin, M. Piel, Y. Chen, J.-B. Sibarita, and M. Bornens. 2005. The extracellular matrix guides the orientation of the cell division axis. *Nat. Cell Biol.* 7:947–953. https://doi.org/10.1038/ncb1307

Timmons, L., and A. Fire. 1998. Specific interference by ingested dsRNA. *Nature.* 395:854. https://doi.org/10.1038/27579

Tse, Y.C., A. Piekny, and M. Glotzer. 2011. Anillin promotes astral microtubule-directed cortical myosin polarization. *Mol. Biol. Cell.* 22: 3165–3175. https://doi.org/10.1091/mbc.e11-05-0399

Uetake, Y., and G. Sluder. 2004. Cell cycle progression after cleavage failure: mammalian somatic cells do not possess a "tetraploidy checkpoint". *J. Cell Biol.* 165:609–615. https://doi.org/10.1083/jcb.200403014

Verbrugghe, K.J.C., and J.G. White. 2004. SPD-1 is required for the formation of the spindle midzone but is not essential for the completion of cytokinesis in C. elegans embryos. *Curr. Biol.* 14:1755–1760. https://doi.org/10.1016/j.cub.2004.09.055

Wagner, E., and M. Glotzer. 2016. Local RhoA activation induces cytokinetic furrows independent of spindle position and cell cycle stage. *J. Cell Biol.* 213:641–649. https://doi.org/10.1083/jcb.201603025

Watanabe, S., Y. Ando, S. Yasuda, H. Hosoya, N. Watanabe, T. Ishizaki, and S. Narumiya. 2008. mDia2 induces the actin scaffold for the contractile ring and stabilizes its position during cytokinesis in NIH 3T3 cells. *Mol. Biol. Cell.* 19:2328–2338. https://doi.org/10.1091/mbc.e07-10-1086

Werner, M., E. Munro, and M. Glotzer. 2007. Astral signals spatially bias cortical myosin recruitment to break symmetry and promote cytokinesis. *Curr. Biol.* 17:1286–1297. https://doi.org/10.1016/j.cub.2007.06.070

Wolfe, B.A., T. Takaki, M. Petronczki, and M. Glotzer. 2009. Polo-like kinase 1 directs assembly of the HsCyk-4 RhoGAP/Ect2 RhoGEF complex to initiate cleavage furrow formation. *PLoS Biol.* 7:e1000110. https://doi.org/10.1371/journal.pbio.1000110

Wurzenberger, C., M. Held, M.A. Lampson, I. Poser, A.A. Hyman, and D.W. Gerlich. 2012. Sds22 and Repo-Man stabilize chromosome segregation by counteracting Aurora B on anaphase kinetochores. *J. Cell Biol.* 198: 173–183. https://doi.org/10.1083/jcb.201112112

Yokoyama, T., H. Goto, I. Izawa, H. Mizutani, and M. Inagaki. 2005. Aurora-B and Rho-kinase/ROCK, the two cleavage furrow kinases, independently regulate the progression of cytokinesis: possible existence of a novel cleavage furrow kinase phosphorylates ezrin/radixin/moesin (ERM). *Genes Cells.* 10:127–137. https://doi.org/10.1111/j.1365-2443.2005.00824.x

Yüce, O., A. Piekny, and M. Glotzer. 2005. An ECT2-centralspindlin complex regulates the localization and function of RhoA. *J. Cell Biol.* 170:571–582. https://doi.org/10.1083/jcb.200501097

Zhang, D., and M. Glotzer. 2015. The RhoGAP activity of CYK-4/MgcRacGAP functions non-canonically by promoting RhoA activation during cytokinesis. *eLife.* 4:e08898. https://doi.org/10.7554/eLife.08898

Zhao, W.M., and G. Fang. 2005. MgcRacGAP controls the assembly of the contractile ring and the initiation of cytokinesis. *Proc. Natl. Acad. Sci. USA.* 102:13158–13163. https://doi.org/10.1073/pnas.0504145102

Zhu, C., and W. Jiang. 2005. Cell cycle-dependent translocation of PRC1 on the spindle by Kif4 is essential for midzone formation and cytokinesis. *Proc. Natl. Acad. Sci. USA.* 102:343–348. https://doi.org/10.1073/pnas.0408438102

Zhu, C., E. Lau, R. Schwarzenbacher, E. Bossy-Wetzel, and W. Jiang. 2006. Spatiotemporal control of spindle midzone formation by PRC1 in human cells. *Proc. Natl. Acad. Sci. USA.* 103:6196–6201. https://doi.org/10.1073/pnas.0506926103